ORIGINAL PAPER

Applications of geochemical and multivariate statistical approaches for the evaluation of groundwater quality and human health risks in a semi-arid region of eastern Maharashtra, India

Deepali Marghade [ID] · Deepak B. Malpe · N. Subba Rao

Abstract A qualitative approach, including geochemical and multivariate statistical approaches, is applied to evaluate the groundwater quality and human health risk, based on analytical data of 72 samples collected from a semi-arid region of eastern Maharashtra, India. The shifting of hydrochemical type from Ca^{2+}–Na^+–HCO_3^- to Na^+–Ca^{2+}–Cl^- type was observed along different flow paths. The main controlling processes observed from the chemical characterisation of the groundwater are water–rock interactions, dedolomitisation and reverse ion exchange. Simulation analysis (mass transfer) exposes the dissolution of dolomite, gypsum, halite, k-feldspar and CO_2 down the simulated pathways. Around 77% of the total variance was observed from the first three principal component analyses. The high positive loadings of EC, TDS, Na^+, K^+, Ca^{2+}, Cl^-, NO_3^- and SO_4^{2-} of PC1 revealed silicate weathering and reverse ion exchange followed by human activities as the contamination sources. The sources identified for high positive loadings on HCO_3^- and SO_4^{2-} of PC2 are soil CO_2 and human activities. The high loadings of pH and F^- in PC3 revealed fluorite dissolution and calcite precipitation. The human health risk calculated for NO_3^- revealed that 58% and 44% of the total groundwater samples surpassed the tolerance limit for non-carcinogenic risk of 1.0 in children and adults. The human health risk assessment for fluoride showed high hazard index values in 40% and 23% of the total groundwater samples for children and adults, respectively. The study suggests some management measures for protection of groundwater resources.

Keywords Geochemical modelling · Mass transfer · Principal component analysis · Health risk estimation · Groundwater quality · India

D. Marghade (✉)
Department of Applied Chemistry, Priyadarshini Institute of Engineering and Technology, Nagpur, India
e-mail: deepalichem@gmail.com

D. B. Malpe
Department of Geology, R.T.M. Nagpur University, Nagpur, India

N. Subba Rao
Department of Geology, Andhra University, Visakhapatnam 530 003, India

Introduction

In semi-arid and arid areas, where precipitation is rare and evaporation is very high, groundwater becomes the most imperious water resource. Groundwater is very imperative in maintaining ecosystems during socio-economic development (Li et al. 2018a; Subba Rao et al. 2019a; Wu et al. 2019a). The rigorous extraction of groundwater, decreased rainfall frequency and decline in its natural restoration capacity

inevitably intensify the groundwater depression. Simultaneously, the groundwater pollution becomes noxious because of the migration of solutes by hydrodynamic dispersion from where the solute amalgamated in aquifers groundwater (Freeze and Cherry 1979). Various water quality crises subsist in surface water and groundwater in India, where 85% of the total rural population depend upon the groundwater resources (Nagaraju et al. 2016). The perturbation of toxic pollutants such as heavy metals, arsenic, nitrate and fluoride distresses the quality of groundwater in India (Marghade et al. 2012; Rina Kumar et al. 2018; Subba Rao et al. 2019b). Numerous studies have been carried out to determine the sources for pollutants such as fluoride, arsenic, heavy metal, landfill leachate, sea water intrusion and industrial effluents throughout India (Marghade et al. 2010; Brindha and Elango 2013; Karunanidhi et al. 2013; Selvam 2014; Singaraja et al. 2014; Brindha et al. 2016, Subba Rao et al. 2017; Duraisamy et al. 2018; Anand et al. 2019; Subba Rao and Chaudhary 2019; Aravinthasamy et al. 2019).

The water dearth distracts the attention of researchers towards sustainable water resources management instead of source appointment of pollutants. The most important step for the sustainable water resources management is understanding the mechanism of natural circulation processes including geochemical processes (composition of soil and rock through which the groundwater drifts, contact time and contact surface between groundwater, mixing, ion exchange), climatic factors (precipitation and evaporation) and unnatural sources (irrigation runoff and industrial and domestic sewage discharge) which govern the groundwater quality during its movement from the recharge to discharge areas (Li et al. 2017).

Now, researchers have concentrated on geochemical characterisation, using various graphical and mathematical modelling approaches. Multivariate statistical evaluation (cluster analysis and principal component analysis) along with geochemical modelling (graphical tools, Pearson's correlation, chloro-alkaline indices, thermodynamic calculations, etc.) has been successfully applied in numerous hydrogeochemical studies (Thilagavathi et al. 2015: Karunanidhi et al. 2014; Marghade et al. 2015; Magesh et al. 2016; Subba Rao 2017a, b, c; Adimallaa et al. 2018; Rina Kumar et al. 2018; Sreedevi et al. 2018; Li et al. 2019a; Subba Rao et al. 2019a; Wu et al. 2014, 2019b).

Principal component analysis (PCA) helps to compress and arrange large data sets to provide significant understanding. Calculated mass balance by simulation analysis epitomises the alterations of the components along the flow path (Li et al. 2007; Subba Rao et al. 2017). Marghade et al. (2019) carried out a comprehensive study in a semi-arid part of Yavatmal District, Maharashtra, India. The study shows that 55% of groundwater samples have fluoride concentration above the recommended limit which mainly comes from weathering and dissolution of fluorite-, apatite-, and fluoride-rich silicates under the influence of high HCO_3^- and Na^+ contents.

The review of the literature suggests that the factors controlling groundwater chemistry are precipitation, evaporation, chemical composition of soils and rocks through which the groundwater flows, resident time of water with aquifer material, dissolution and ion exchange, domestic waste, irrigation return flow and industrial discharge. For assessing these factors, the multivariate statistical analysis, graphical tools, chloro-alkaline indices and thermodynamic calculations have been widely used.

The earlier study of adjoining region has mainly been focused on fluoride contamination in groundwater and its health impact (Marghade et al. 2019). The detailed geochemical characterisation is very essential for assessing the groundwater quality not only for its present use but also for sustainable development. In this perception, an endeavour has been made to evaluate the factors controlling geochemistry, using geochemical and multivariate approaches. The human health risk assessment has also been carried out which would be helpful for sustainable groundwater resources management.

Study area

The Wani region of Yavatmal district, Maharashtra, India, is located in between 19′53″ to 20′10″ N latitude and 78′4″ to 79′08″ E longitude (Fig. 1a). The area experiences hot summer and mild winter with an annual average temperature range of 15.5–42.0 °C. The annual rainfall in the region is about 850 mm between June and September (CGWB 2013). The drainage pattern is of sub-dendritic (Fig. 1c). The major land-use type in the region is cultivation land.
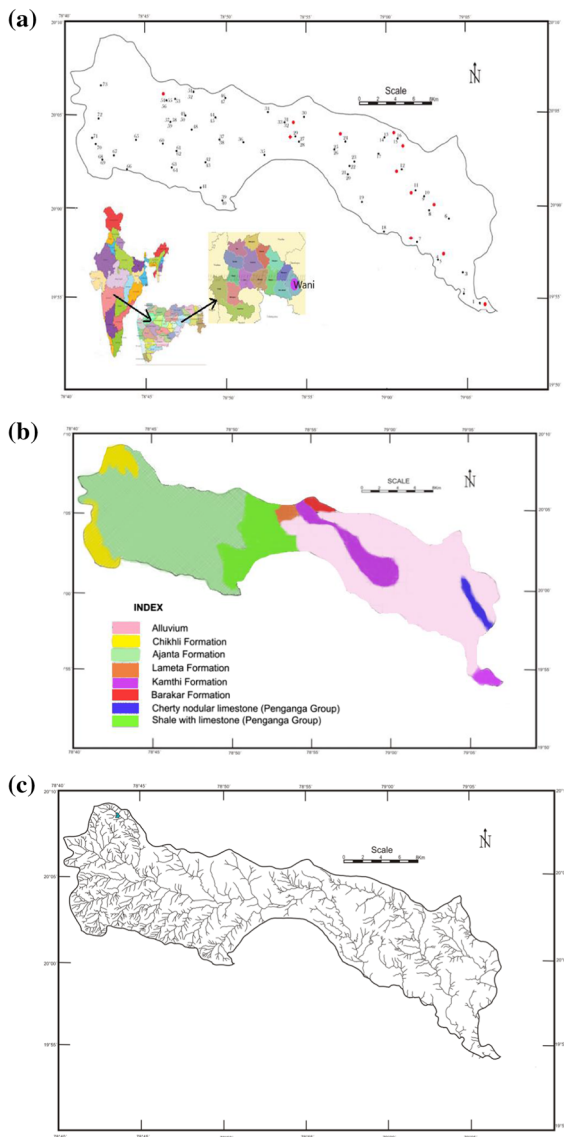
Fig. 1 **a** Location, **b** geological and **c** drainage map of the study region

Geology and hydrogeology

Geologically, the eastern part of the present study region contains Penganga limestones of Neoproterozoic age signified by fluorite-bearing veins at some places (CGWB 2013). The Penganga limestone is overlain by Barakar and Kamthi sandstone formations of Gondwana Supergroup of Permo-Carboniferous age (Fig. 1b). The formation of coal began in carboniferous period. They are most productive water-bearing formations. The Gondwana rocks are

overlain by Lameta Formation represented by clay with cherty limestone and sandstones which are in turn overlain by Cretaceous to Paleogene basalts of Ajanta and Chikhli formations of Sahyadri Group of Deccan Volcanic Provence. Plagioclase feldspar and pyroxence constitute the primary minerals of basalt with secondary quartz, calcite and zeolites. Quaternary alluvium and black soils consisting of silt, clay and sand overlie basalts.

The groundwater is the major source of drinking, while seasonal rainfall is the main source of groundwater recharge. The geographical and geological settings are the major factors for occurrence and distribution of groundwater in the region. Water retention capacity of karstified Penganga limestones, Gondwana sandstones and Quaternary alluvium is prominent. Groundwater occurs under unconfined condition in weathered zones and under semi-confined to confined conditions in fracture zones. The depth to water level varies according to lithology. In Penganga Group rocks, it is 4–16 m below ground level (bgl) during pre-monsoon and 2.3–7.6 m bgl during post-monsoon period. In Gondwana, it varies from 7.5 to 3.6 m bgl during pre- and post-monsoon seasons, respectively, while in Deccan Traps, it varies from 2.1 to 7.6 m bgl during pre- and 1.3–5.7 m bgl during post-monsoon season. The drainage map of the present study region is given in Fig. 1c. Evapotranspiration and artificial extraction are the main discharge pathways of groundwater.

Groundwater sampling and analytical procedure

Seventy-two bore wells of the study region which are used for drinking and irrigation purposes without any treatment are selected and sampled. The physico-chemical parameters of groundwater are analysed following the standard procedure of American Public Health Association (APHA 1999). The physical parameters pH and electrical conductivity (EC) are measured onsite by respective meters. Calcium (Ca^{2+}) and magnesium (Mg^{2+}) are determined volumetrically with standard ethylene diamine tetra acetic acid. Chloride (Cl^-) is determined, using standard solution of silver nitrate. Carbonate (CO_3^{2-}) and bicarbonate (HCO_3^-) are determined by titrating with standard HCl solution. Sodium (Na^+) and potassium (K^+) are measured by flame photometric method. Fluoride

(F⁻), sulphate (SO_4^{2-}) and nitrate (NO_3^-) are determined, using UV–visible spectrophotometer. The ionic data are used to calculate total dissolved solids (TDS). The precision of the chemical analyses is carefully checked by taking duplicate samples. The ionic balance errors for the analyses are within ± 5% level.

Modelling methods

The Microsoft Excel 2007 was used to perform statistical analysis of data obtained after analysis. The bivariate diagrams are used to recognise the reactions between groundwater and the aquifer matrix (Kshetrimayum 2015). To comprehend the data set obtained from the study region, Pearson's correlation coefficient method and principal component analysis are used.

Geochemical modelling is used for studying hydrochemical evolution mechanisms. The PHREEQC software is used to compute saturation index (SI) values of minerals. Inverse geochemical modelling is also computed by using PHREEQC interactive software, which is used to compute the number of moles of minerals and gases transferred from dissolved state to precipitated/degassed from the solutions (Li et al. 2010; Subba Rao et al. 2017). For calculation of mass balance, the differences in compositions between the initial and final end-member solutions have been used. PCA was performed by using varimax rotation method with Kaiser normalisation (Hussin et al. 2016; Subba Rao et al. 2017).

Health risk assessment

Human health risk assessment is the technique to evaluate the nature and possibility of ill-health effects in humans who consumed contaminated groundwater regularly (Adimallaa and Qian 2019; Li et al. 2016a, 2019b). In this study, drinking water consumption was the major exposure pathway for nitrate and fluoride. The IRIS (Integrated Risk Information System) model introduced by US Environmental Protection Agency (USEPA 2004) is used to measure the exposure dose (E) through ingestion pathway and probable non-carcinogenic risk of hazard quotient or hazard index (HQ) (He and Wu 2019; He et al. 2019; Karunanidhi et al. 2019):

$$E = \frac{CPW \times IR \times ED \times EF}{ABW \times AET} \tag{1}$$

$$HQ = \frac{E}{RfD} \tag{2}$$

where E is the chronic daily intake (mg/kg/day), CPW is the concentration of a particular contaminant in groundwater (mg/L), IR is the human ingestion rate (2.5 L/day for adults, 0.78 L/day for children), ED is the exposure duration (years: 64 and 12 for adults and children), EF is the exposure frequency(days/years: 365 days), ABW is the average body weight (Kg: 57.5 and 18.7 for adults and children, respectively), AET is the average time (days: 23,360 and 4380 for adults and children), HQ is the non-carcinogenic for hazard quotient and RfD is the reference dose of fluoride and nitrate 4.00E − 02 and 1.1E + 00 mg/kg-day, respectively (Integrated Risk Information System, USEPA 2004).

Hazard index interprets 10^{-6} risk level for carcinogens, and HQ is 1 for non-carcinogens. If a person is exposed daily for a lifetime to 1 μg of the nitrate/fluoride per litre of drinking water, the unit risk = 2×10^{-6} per μg/L, meaning two excess cancer cases are expected to develop per 1000,000 people.

Results and discussion

General groundwater chemistry

Groundwater of study region is neutral to slightly alkaline (pH 6.7–8.6). A total dissolved solid (TDS) diverges from 240.8 to 4139.8 mg/L with an average of 1056.3 mg/L (Table 1).

About 21% of sampling points exceed maximum permissible limit of 1500 mg/L marking them not recommended for drinking purposes (Marghade et al. 2015; Subba Rao 2017b). The dominant Na⁺ level in the groundwater diverges from 7.4 to 1364 mg/L with a mean of 221 mg/L. Almost 40% of sampling points have Na⁺ concentration above the prescribed limit of 200 mg/L (Table 1). The amount of K⁺, Ca²⁺ and Mg²⁺ in the sampling points diverges in the ranges of 0–201, 10–364, 1.2–153.1 mg/L, respectively.

HCO_3^- is the dominant anion over other anions and diverges from 103.7 to 1159 mg/L (Table 1). High HCO_3^- concentration in groundwater reduces the

Table 1 Analytical data of groundwater samples (n = 72)[a]

No.	pH	Electrical conductivity (μS/cm)	Total dissolved solids (mg/l)	Concentration of ions								
				Sodium (mg/l)	Potassium (mg/l)	Calcium (mg/l)	Magnesium (mg/l)	Bicarbonate (mg/l)	Chloride (mg/l)	Sulphate (mg/l)	Nitrate (mg/l)	Fluoride (mg/l)
1	7.1	3440	2104.9	268.0	42.0	220	109.4	152.5	440.2	145.5	803.0	0.6
2	7.3	830	527.1	110.0	40.0	38	26.7	451.4	21.3	55.5	9.9	0.0
3	7.1	1230	697.6	111.0	41.0	62	29.2	451.4	85.2	123.7	19.4	0.4
4	6.8	5250	2929.2	758.0	92.0	206	79.0	311.1	880.4	287.6	470.0	0.7
5	7.4	740	467.4	43.0	8.2	52	63.2	256.2	81.7	73.2	17.7	0.3
6	7.3	1150	874.8	206.0	21.0	44	45.0	262.3	174.0	75.7	177.8	0.2
7	7.1	2740	1889.4	596.0	32.0	106	20.7	500.2	397.6	189.0	297.5	0.5
8	6.7	3790	2291.8	239.0	36.0	326	127.6	146.4	759.7	135.0	595.0	0.3
9	7	1520	1017.7	196.0	32.0	164	17.0	353.8	202.4	102.9	126.0	0.5
10	7.2	1740	1053.2	267.0	27.0	112	10.9	500.2	266.3	82.0	37.4	0.6
11	6.7	4750	2678.6	542.0	53.0	272	105.7	219.6	859.1	177.0	559.4	0.6
12	6.8	3670	2356.5	478.0	156.0	136	136.1	298.9	685.2	317.0	297.5	1.3
13	7.2	2200	1428.9	367.0	43.0	94	64.4	311.1	379.9	292.4	31.6	1.1
14	7.5	2050	1262.0	324.0	53.0	84	57.1	518.5	298.2	102.6	82.9	1.0
15	6.9	4410	2851.4	439.0	56.0	348	153.1	274.5	781.0	178.6	758.0	0.4
16	7.2	2790	1772.4	389.0	67.0	210	18.2	207.4	415.4	193.1	375.6	0.4
17	8.4	940	731.2	250.0	26.0	40	3.6	250.1	195.3	72.4	17.5	1.4
18	7.1	1320	926.2	279.0	32.0	38	27.9	433.1	113.6	146.7	72.2	0.2
19	6.9	390	240.8	12.3	5.2	36	29.2	158.6	39.1	35.1	4.2	0.5
20	7.4	2350	1425.5	356.0	41.0	52	76.5	536.8	347.9	91.6	191.3	0.8
21	6.9	1740	1099.1	311.0	15.7	40	58.3	542.9	134.9	140.3	126.7	0.8
22	7	860	489.9	25.5	1.3	82	58.3	219.6	110.1	42.4	59.5	1.0
23	7.8	1160	555.6	89.2	2.1	56	81.4	207.4	120.7	62.9	38.7	0.8
24	7.8	3450	2909.0	1364.0	72.0	76	99.6	372.1	603.5	356.2	150.0	1.6
25	7.1	1240	821.3	212.0	38.0	56	36.5	451.4	145.6	60.7	46.5	0.4
26	7.1	1420	751.8	119.0	44.0	46	62.0	414.8	152.7	88.1	31.9	0.7
27	7.2	920	523.4	54.3	5.8	36	82.6	408.7	42.6	57.2	40.0	0.6
28	7.1	1430	1012.4	268.0	45.0	58	30.4	317.2	205.9	62.2	183.9	0.4
29	7.1	2260	1511.4	331.0	41.0	114	58.3	420.9	316.0	60.1	380.0	0.6
30	7.6	2170	1185.3	352.0	45.0	40	41.3	524.6	308.9	57.2	77.0	1.7
31	7.9	8140	4139.8	1221.0	104.0	364	23.1	1159	887.5	925.0	35.0	0.7

Table 1 continued

| No. | pH | Electrical conductivity (µS/cm) | Total dissolved solids (mg/l) | Concentration of ions | | | | | | | | | | |
				Sodium (mg/l)	Potassium (mg/l)	Calcium (mg/l)	Magnesium (mg/l)	Bicarbonate (mg/l)	Chloride (mg/l)	Sulphate (mg/l)	Nitrate (mg/l)	Fluoride (mg/l)
32	7.8	4160	2781.7	835.0	62.0	178	20.7	128.1	1136.0	184.6	300.2	1.1
33	7.8	1940	1358.9	469.0	45.0	34	7.3	481.9	298.2	148.6	114.0	1.8
34	7.6	1110	732.8	36.6	18.4	86	76.5	317.2	227.2	37.0	92.1	0.4
35	7.2	1020	623.9	17.9	34.6	54	92.3	335.5	92.3	89.9	73.9	1.2
36	7.2	670	362.5	21.8	11.2	56	26.7	219.6	74.6	44.0	17.9	0.5
37	7.2	870	509.2	44.3	2.1	46	57.1	396.5	67.5	47.9	45.5	0.6
38	7.3	1340	1002.4	149.0	201.0	42	34.0	274.5	181.1	60.1	197.3	0.7
39	7.2	1190	623.1	27.0	9.0	112	70.5	323.3	134.9	51.9	55.8	0.4
40	7.4	740	369.2	30.9	2.1	86	41.3	183	32.0	43.7	40.9	0.9
41	7.1	1240	647.1	131.0	48.0	146	55.9	103.7	113.6	52.2	48.3	0.2
42	7.7	700	387.9	21.3	3.6	48	48.6	237.9	56.8	42.6	47.6	0.5
43	7.6	1100	723.4	38.6	47.3	76	68.0	262.3	149.1	54.2	158.0	0.9
44	7.6	1550	928.7	196.0	41.0	102	30.4	280.6	287.6	60.7	70.2	0.6
45	7.8	1900	1057.5	216.0	43.0	84	76.5	372.1	351.5	95.0	5.2	0.3
46	7.5	1050	555.9	46.8	4.1	72	59.5	292.8	74.6	60.1	91.9	0.5
47	7.8	950	548.9	42.3	3.8	70	58.3	262.3	103.0	58.6	81.1	0.7
48	7.6	580	284.9	18.9	1.7	38	35.2	176.9	24.9	42.6	34.6	0.6
49	7.6	840	499.6	84.2	0.2	42	49.8	353.8	21.3	40.4	83.3	1.5
50	7.7	870	526.0	35.3	0.1	80	55.9	213.5	99.4	55.5	92.4	0.7
51	7.4	1720	1106.4	164.0	41.0	144	58.3	323.3	291.1	69.9	176.0	0.5
52	7.5	1470	1134.8	175.0	44.0	136	45.0	274.5	276.9	85.0	235.3	0.4
53	7.5	810	483.1	32.1	0.4	38	64.4	311.1	74.6	55.8	61.1	1.2
54	8.1	4230	2331.9	525.0	41.0	150	114.2	384.3	884.0	186.2	238.2	1.2
55	7.7	2340	1943.7	526.0	62.0	146	36.5	317.2	571.6	108.1	333.6	1.4
56	7.8	6900	658.8	121.0	29.0	50	52.2	396.5	88.8	39.8	78.7	1.0
57	7.6	750	457.0	41.1	37.1	56	31.6	280.6	74.6	43.7	32.2	0.5
58	7.8	820	479.6	21.9	74.7	56	41.3	341.6	60.4	42.8	11.0	0.7
59	8	780	450.8	33.6	59.1	40	52.2	335.5	39.1	39.4	18.8	0.8
60	7.6	610	367.6	35.2	5.8	88	8.5	213.5	24.9	51.8	45.8	0.9
61	7.5	900	595.0	49.1	6.1	84	53.5	311.1	110.1	55.5	80.5	0.8
62	7.9	970	641.1	28.5	2.9	78	70.5	176.9	149.1	77.9	145.0	0.8

Table 1 continued

No.	pH	Electrical conductivity (μS/cm)	Total dissolved solids (mg/l)	Concentration of ions								
				Sodium (mg/l)	Potassium (mg/l)	Calcium (mg/l)	Magnesium (mg/l)	Bicarbonate (mg/l)	Chloride (mg/l)	Sulphate (mg/l)	Nitrate (mg/l)	Fluoride (mg/l)
63	7.4	600	390.3	38.1	5.1	44	34.0	298.9	74.6	39.4	5.3	0.3
64	8.1	1630	1137.9	154.0	46.0	170	43.7	250.1	259.2	91.9	247.4	0.6
65	8.1	1350	945.7	365.0	37.0	24	7.3	280.6	295.0	73.6	1.6	1.9
66	7.4	960	525.3	62.1	0.7	68	60.8	280.6	95.0	52.8	45.2	0.5
67	7.7	750	473.8	27.5	0.0	62	60.8	262.3	42.6	44.1	105.2	0.6
68	8.6	610	415.0	136.0	1.1	10	1.2	176.9	42.6	46.3	87.7	1.6
69	8	670	337.9	7.4	4.3	40	58.3	262.3	17.8	39.4	39.2	0.4
70	8	660	344.2	57.8	4.3	46	24.3	213.5	56.8	44.0	3.5	0.7
71	7.4	1100	636.1	29.9	2.6	164	24.3	213.5	117.2	76.4	114.9	0.1
72	7.6	1780	1151.4	241.0	35.0	128	30.4	207.4	312.4	77.5	222.0	1.4
Min	6.7	390.0	240.8	7.4	0.0	10.0	1.2	103.7	17.8	35.1	1.6	0.0
Max	8.6	8140.0	4139.8	1364.0	201.0	364.0	153.1	1159.0	1136.0	925.0	803.0	1.9
Average	7.5	1782.2	1056.3	221.0	33.8	95.6	52.4	318.9	249.1	104.2	140.2	0.7
SD	0.4	1483.1	802.5	261.6	34.7	74.5	31.2	145.5	256.2	119.9	168.5	0.4
CV (%)	5.3	83.2	76.0	118.4	102.6	78.0	59.6	45.6	102.9	115.1	120.2	56.7

[a]All hydrochemical values are expressed in mg/L except pH and electrical conductivity (EC) in micro-Siemen per centimetre

available adsorption sites of the sorbents that lead to the release of fluoride from minerals (Subba Rao 2017a). The semi-arid climate-induced prolonged evaporative enrichment of water leads to high Cl^- concentration (Subba Rao 2006). Chloride varies from 17.8 to 1136 mg/L. SO_4^{2-} in groundwater ranges from 35.1 to 925 mg/L. The high SO_4^{2-} concentration may be due to geogenic processes and high evaporation rate in the study region (Adimallaa and Qian 2019). The elevated nitrate (1.6–803 mg/L with an average of 140.2 mg/L) concentrations in drinking water cause fatal disease "blue baby syndrome" (*methaemoglobinemia*) in infants (Marghade et al. 2011; Subba Rao 2017b). About 66.6% of the groundwater samples were found to surpass the tolerance limit of 45 mg/L for nitrate (WHO 2011). It is observed that samples having high TDS have high concentration of Na^+ and NO_3^-. This strongly shows that the groundwater quality is influenced by human activities and mainly by irrigation return flows, drainage effluents and animal waste. The 0.5–1.5 mg/L of fluoride in drinking water is a very essential element for human health (WHO 2011), but its higher concentration becomes risky for human health. Only 12% of the groundwater samples contain the F^- concentration above 1.5 mg/L. (Table 1).

The divergences in the standard deviation values (0.4–1483) (Table 1) due to various hydrogeochemical reactions indicate a varied distribution of salts in the groundwater (Subba Rao et al. 2017). The difference in the coefficient of variation values also shows a varied distribution of the chemical variables in groundwater. The highest coefficient of variation is of NO_3^- (120.4%) followed by Na^+ (118.4%), SO_4^{2-} (115.1%) and Cl^- (102.9%). pH has lowest coefficient of variation (5.3%). This observation suggests that Na^+ and NO_3^- may be the main key factors in controlling groundwater chemistry.

The Pearson's correlation coefficient method generates matrix with significant correlations between the parameters. The electrical conductivity shows high correlation coefficient with Ca^{2+}, Na^+, Cl^- and SO_4^{2-}, which elucidates large involvement of these elements to the groundwater chemistry. Significant positive correlation (Table 2) observed between TDS and Na^+, Ca^{2+}, Cl^- and SO_4^{2-} indicates contribution of these ions towards hydrochemical characteristics of groundwater (Tay et al. 2017). Strong positive correlation of Na^+ with Cl^- ($r = 0.81$) and SO_4^{2-} ($r = 0.80$) indicates high pollution level of groundwater (Table 2). This is further supported by strong positive correlation of Ca^{2+} with Cl^- ($r = 0.75$) and NO_3^- ($r = 0.72$). An alkaline environmental condition due to high bicarbonate concentration (positive correlation of F^- with pH, $r = 0.43$) promotes F^- leaching (Subba Rao 2003, 2011).

A significant low correlation between K^+ and NO_3^- ($r = 0.34$) and SO_4^{2-} ($r = 0.48$) indicates the presence of other sources of these ions irrespective of fertiliser runoff (Table 2). Negative correlation between F^- and Ca^{2+} ($r = -0.18$) is endorsed for the influencing

**Table 2** Correlation coefficients matrix

	pH	EC	TDS	Na^+	K^+	Ca^{2+}	Mg^{2+}	HCO_3^-	Cl^-	SO_4^{2-}	NO_3^-
pH	1.00										
EC	− 0.13	1.00									
TDS	− 0.19	**0.86**	1.00								
Na^+	− 0.02	**0.75**	**0.90**	1.00							
K^+	− 0.17	0.49	0.59	0.53	1.00						
Ca^{2+}	− 0.31	**0.70**	**0.78**	0.50	0.34	1.00					
Mg^{2+}	− 0.35	0.33	0.37	0.13	0.16	0.39	1.00				
HCO_3^-	0.00	0.42	0.37	0.46	0.26	0.10	− 0.11	1.00			
Cl^-	− 0.15	**0.81**	**0.95**	**0.81**	0.53	**0.75**	0.39	0.18	1.00		
SO_4^{2-}	− 0.05	**0.74**	**0.80**	**0.80**	0.48	0.59	0.14	**0.62**	**0.65**	1.00	
NO_3^-	− 0.39	0.54	**0.67**	0.38	0.34	**0.72**	0.53	− 0.18	**0.67**	0.22	1.00
F^-	0.43	0.15	0.17	0.33	0.14	− 0.18	− 0.07	0.07	0.20	0.13	− 0.05

Bold numbers indicates strong positive correlation between two parameters

Fig. 2 Piper plot
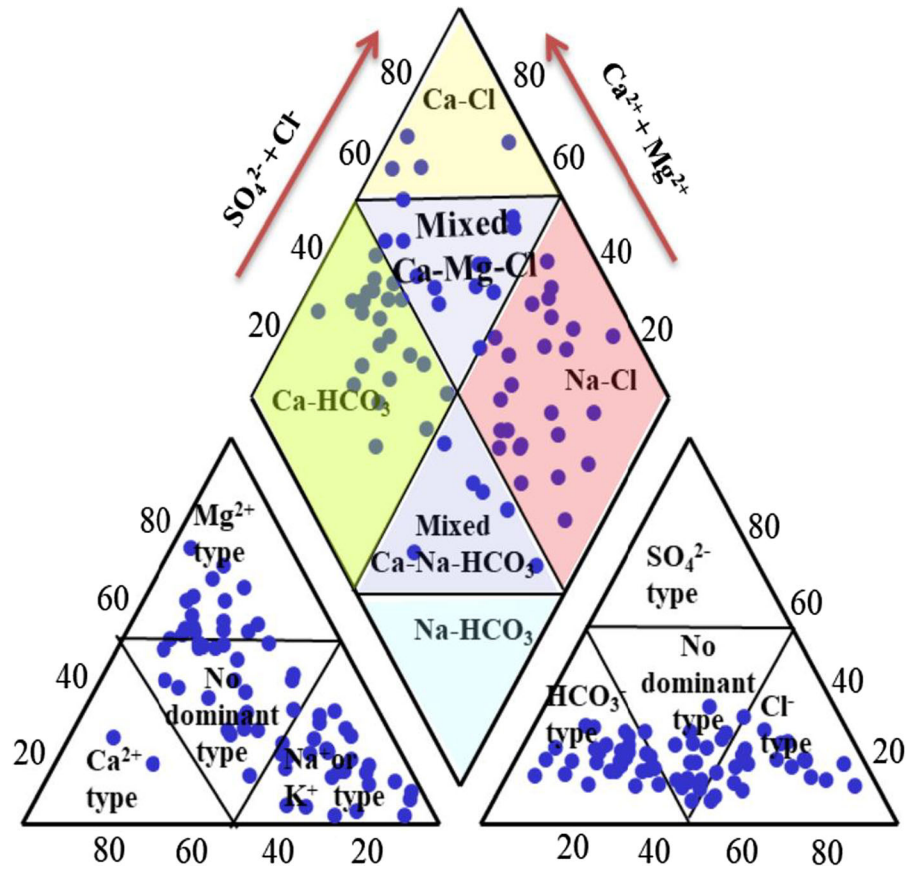
factors for fluorite (CaF_2) dissolution in groundwater and the removal of Ca^{2+} from groundwater through the precipitation of CaF_2 due to high load of Ca^{2+} in groundwater (Subba Rao et al. 2013). The Na^+-enriched groundwater samples contain high F^- concentration which is supported by positive correlation ($r = 0.33$) between F^- and Na^+. The high R^2 value than HCO_3^- confirmed the significant contribution of Na^+ in controlling the groundwater F^- geochemistry (Magesh et al. 2016; Subba Rao 2017a, c). The less significant positive correlation between F^- and K^+ ($r = 0.14$) and negative correlation between F^- and NO_3^- ($r = -0.05$) indicate less contribution of anthropogenic input such as fertilisers and domestic waste in enrichment of F^- in the study region.

Groundwater types

The sequence of cation dominance is $Na^+ > K^+ > Ca^{2+} > Mg^{2+}$ and anion dominance is $HCO_3^- > Cl^- > SO_4^{2-} > NO_3^- > F^-$ in the groundwater of the study region. The groundwater types derived from the major ion chemistry are represented in trilinear plot (Fig. 2) (Piper 1944). About 38% of sampling points fall in Na–Cl and 32% in Ca–HCO_3 water-type zones. Mixed water types Ca–Mg–Cl and Ca–Na–HCO_3 are observed in 8 and 15% of the total samples. It is interpreted that the freshwater (Ca–HCO_3) shifts towards the saline water (Na–Cl) through the mixed water (Ca–Mg–Cl and Ca–Na–HCO_3), indicating the influence of geogenic and human activities on the groundwater chemistry (Fig. 2).

Risk assessment for human health

The non-carcinogenic health risk for adults and children is due to the consumption of polluted drinking water. The risks are calculated by IRIS model for those samples which contain high NO_3^- and F^- in the study region (Table 3).

As nitrate is a non-geogenic contaminant, it is considered as an indicative of anthropogenic activities

Table 3 Calculated health risk from nitrate and fluoride pollution for adult and children

Sample ID	NO$_3^-$ concentration	Total HQ for child	Total HQ for adult	F$^-$ concentration	Total HQ for child	Total HQ for adult
1	803	1.01E + 01	6.05E + 00	0.6	7.51E − 01	4.52E − 01
4	470	5.88E + 00	3.54E + 00	0.7	8.76E − 01	5.27E − 01
6	177.8	2.23E + 00	1.34E + 00	0.2	2.50E − 01	1.51E − 01
7	297.5	3.72E + 00	2.24E + 00	0.5	6.26E − 01	3.77E − 01
8	595	7.45E + 00	4.48E + 00	0.3	3.76E − 01	2.26E − 01
9	126	1.58E + 00	9.49E − 01	0.5	6.26E − 01	3.77E − 01
11	559.4	7.00E + 00	4.21E + 00	0.6	7.51E − 01	4.49E − 01
12	297.5	3.72E + 00	2.24E + 00	1.3	1.88E + 01	1.13E + 01
13	31.6	3.88E − 01	2.34E − 01	1.1	1.38E + 00	8.29E − 01
14	82.9	1.04E + 00	6.25E − 01	1	1.25E + 00	7.53E − 01
15	758	9.49E + 00	5.71E + 00	0.4	5.01E − 01	3.01E − 01
16	375.6	4.71E + 00	2.83E + 00	0.4	5.01E − 01	3.01E − 01
17	17.5	2.19E − 01	1.32E − 01	1.4	1.75E + 00	1.05E + 00
18	72.2	9.01E − 01	5.42E − 01	0.2	2.50E − 01	1.51E − 01
20	191.3	2.39E + 00	1.44E + 00	0.8	1.00E + 00	6.03E − 01
21	126.7	1.59E + 00	9.57E − 01	0.8	1.00E + 00	6.03E − 01
22	59.5	7.51E − 01	4.52E − 01	1	1.25E + 00	7.53E − 01
23	38.7	4.88E − 01	2.94E − 01	0.8	1.00E + 00	6.03E − 01
24	150	1.88E + 00	1.13E + 00	1.6	2.00E + 00	1.21E + 00
27	40	5.01E − 01	3.01E − 01	0.6	1.00E + 00	1.00E + 00
28	183.9	2.30E + 00	1.39E + 00	0.4	5.01E − 01	3.01E − 01
29	380	4.76E + 00	2.86E + 00	0.6	7.51E − 01	4.52E − 01
30	77	9.64E − 01	5.80E − 01	1.7	2.13E + 00	1.28E + 00
32	300.2	3.76E + 00	2.26E + 00	1.1	1.38E + 00	2.90E − 02
33	114	1.43E + 00	8.59E − 01	1.8	2.25E + 00	1.36E + 00
34	92.1	1.15E + 00	6.93E − 01	0.4	5.01E − 01	3.01E − 01
35	73.9	9.27E − 01	5.57E − 01	1.2	1.88E + 00	1.13E + 00
38	197.3	2.47E + 00	1.48E + 00	0.7	3.76E − 01	2.26E − 01
43	158	1.98E + 00	1.19E + 00	0.9	1.13E + 00	6.78E − 01
44	70.2	8.79E − 01	5.29E − 01	0.6	7.51E − 01	4.52E − 01
46	91.9	1.15E + 00	6.93E − 01	0.5	6.26E − 01	3.77E − 01
47	81.1	1.01E + 00	6.10E − 01	0.7	8.76E − 01	5.27E − 01
49	83.3	1.04E + 00	6.25E − 01	1.5	1.88E + 00	1.13E + 00
50	92.4	1.15E + 00	6.93E − 01	0.7	8.76E − 01	5.27E − 01
51	176	2.20E + 00	1.33E + 00	0.5	6.26E − 01	3.77E − 01
52	235.3	2.94E + 00	1.77E + 00	0.4	5.01E − 01	3.01E − 01
53	61.1	7.64E − 01	4.60E − 01	1.2	1.50E + 00	9.04E − 01
54	238.2	2.98E + 00	1.79E + 00	1.2	1.50E + 00	9.04E − 01
55	333.6	4.18E + 00	2.52E + 00	1.4	1.75E + 00	1.05E + 00
56	78.7	9.89E − 01	5.95E − 01	1.0	1.25E + 00	7.53E − 01
61	80.5	1.01E + 00	6.06E − 01	0.8	1.00E + 00	6.03E − 01
62	145	1.82E − 01	1.09E − 01	0.8	1.00E + 00	6.03E − 01
64	247.4	3.09E − 01	1.86E − 01	0.6	7.51E − 01	4.52E − 01
65	1.6	2.00E − 02	1.21E − 02	1.9	2.38E + 00	1.43E + 00

Table 3 continued

Sample ID	NO_3^- concentration	Total HQ for child	Total HQ for adult	F^- concentration	Total HQ for child	Total HQ for adult
67	105.2	1.31E + 00	7.91E − 01	0.6	7.51E − 01	4.52E − 01
68	87.7	1.10E + 00	6.63E − 01	1.6	2.00E + 00	1.21E + 00
71	114.9	1.44E + 00	8.66E − 01	0.1	1.25E − 01	7.53E − 02
72	222	2.78E + 00	1.67E + 00	1.4	1.75E + 00	1.05E + 00
min	1.6	2.00E − 02	1.21E − 02	0.1	1.25E − 01	2.90E − 02
Max	803	1.01E + 01	6.05E + 00	1.9	1.88E + 01	1.13E + 01
Average	195.7	2.36E + 00	1.42E + 00	0.85	1.43E + 00	8.53E − 01

such as manures, animal wastes and agricultural runoff (Marghade et al. 2011). The NO_3^- concentration varies from 1.2 to 803 mg/L in groundwater of the study region. About 67% of the total groundwater samples have NO_3^- concentration above the tolerance limit of 45 mg/L (WHO 2011). The health risk values for nitrate range from 2.00E − 02 to 1.01E + 01 with an average of 2.36E + 00 calculated for children (Table 3). For adults, HQ values for nitrate vary from 1.21E − 02 to 6.05E + 01 with an average of 1.42E + 00. In 22% and 7% of the total groundwater samples, HQ has very high (> 3) non-carcinogenic risk for nitrate for children and adults, respectively. The values, which are higher for children, are due to prolonged drinking of nitrate-contaminated water, causing blue baby syndrome in children of the study region. The health risks assessment also revealed that 58% and 44% of the total groundwater samples exceed the tolerance limit of 1.0E + 00 prescribed for non-carcinogenic risk in children and adults, respectively (Table 3).

Similarly, for fluoride, calculated HQ values are higher than the reference dose of 1.0E + 00 mg/kg-day in 19 (40%) and 11 (23%) of the total groundwater samples for children and adults, respectively, increasing the probability of dental and skeletal fluorosis (Table 3). The high-risk values for fluoride in 12% of the total groundwater samples are due to concentration of fluoride above the prescribed limit of 1.5 mg/L.

Processes regulating groundwater chemistry

Various factors such as geogenic, ion exchange, anthropogenic and climatic conditions are accountable for hydrogeochemical amendment of groundwater chemistry

Carbonates and gypsum dissolution

The value of Ca^{2+}/Mg^{2+} molar ratio equal to one indicates the dissolution of dolomite and more than one indicates higher calcite contribution and release of Ca^{2+} ions into the groundwater during recharging of aquifer (Fig. 3a). The Ca^{2+}/Mg^{2+} molar ratio greater than one specifies the dominance of calcite dissolution over dolomite dissolution in the groundwater. However, the dispersion of sampling points above and below the uniline of 1:1 verifies the existence of calcite and dolomite dissolution in the groundwater, but neglects the dominancy of any single process (Wu et al. 2019a). The contribution of carbonate (such as calcite $CaCO_3$ and dolomite $CaMg (CO_3)_2$ to hydrochemistry is significantly indicated by $(Ca^{2+} + Mg^{2+})$ and $(HCO_3^- + SO_4^{2-})$ bivariate plot (Fig. 3b). Most of the groundwater samples fall along the 1:1 line, indicating the dominance of carbonate component. The dispersal of groundwater sampling points from equiline indicates the contribution of cation exchange and/or the dissolution of silicate for high Ca^{2+} and Mg^{2+} percentage in the groundwater. However, all groundwater samples fall above the 1:1 line in the $(Ca^{2+} + Mg^{2+})$ versus HCO_3^- diagram (Fig. 3c), indicating less dissolution of carbonates (Wu and Sun 2016).

When the aquifer contains both dolomite and calcite, it is possible that the gypsum dissolution accelerates the dedolomitisation process due to simultaneous precipitation of calcite and dissolution of dolomite (Fijani et al. 2017). The dissolution of gypsum tends to increase calcium concentration, causing precipitation of calcite (Li et al. 2016b, c). The maximum number of groundwater sampling points falls above the zero line of binary plot of

Fig. 3 Bivariate plots of **a**
Ca^{2+} and Mg^{2+}, **b**
Ca^{2+} + Mg^{2+} and
HCO$_3^-$ + SO$_4^{2-}$, **c**
Ca^{2+} + Mg^{2+} and HCO$_3^-$, **d**
Ca^{2+} + Mg^{2+} − 0.5 HCO$_3^-$
and SO$_4^{2-}$ and **e** Ca^{2+} and
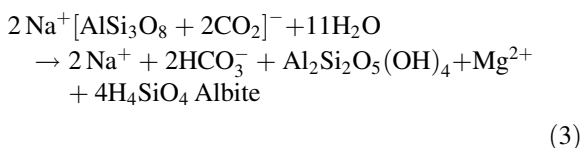SO$_4^{2-}$ **f** Na$^+$ and Cl$^-$ **g** Na$^+$
versus TC
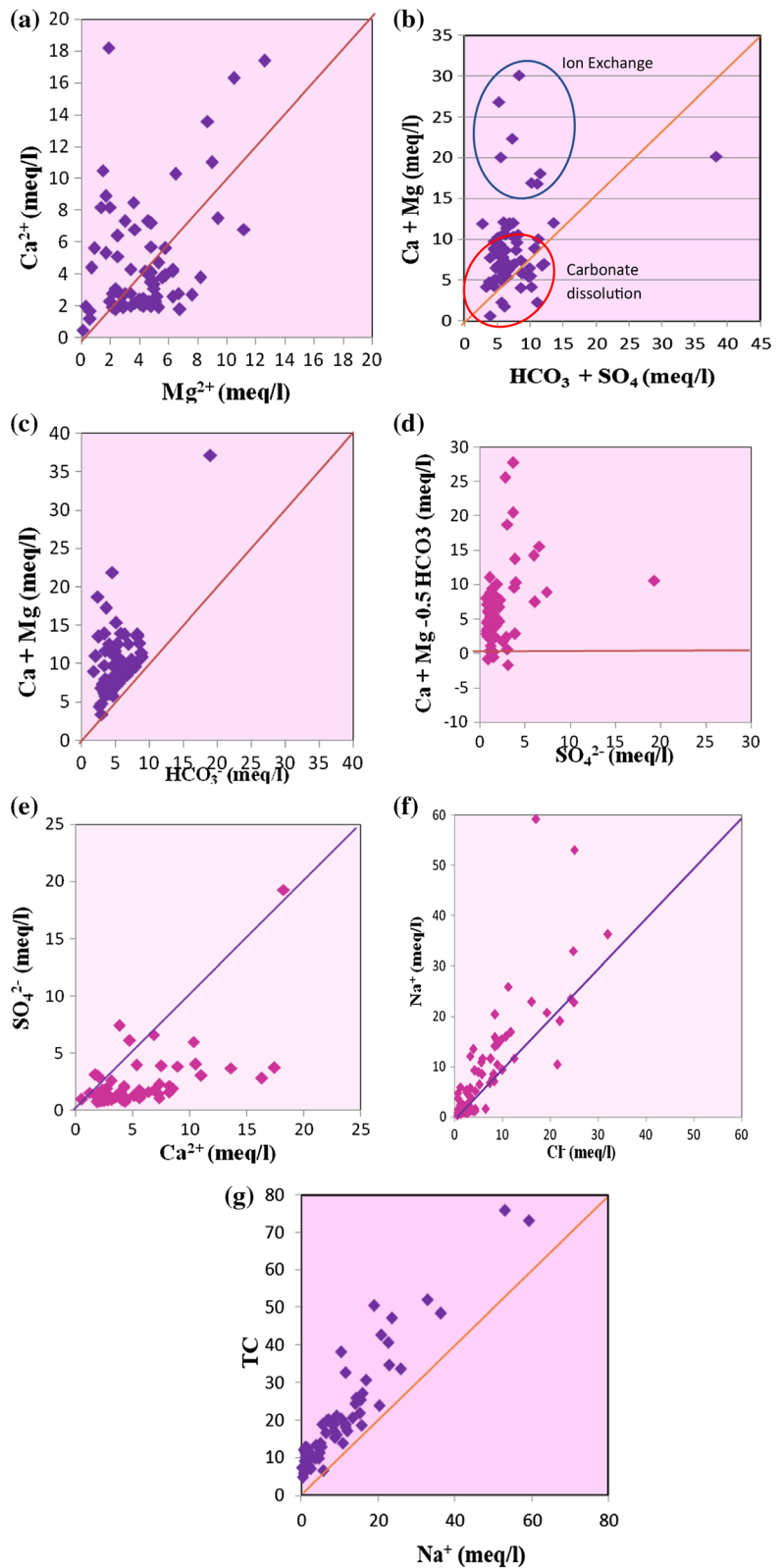
$[(Ca^{2+} + Mg^{2+}) - 0.5 \quad HCO_3^-]$ versus SO_4^{2-} (Fig. 3d), which proves that gypsum is also a source of Ca^{2+} and SO_4^{2-} in the groundwater system (Subba Rao et al. 2019a, b). However, the binary plot between Ca^{2+} and SO_4^{2-} (Fig. 3e) resolved that gypsum dissolution is highly masked by other factors such as recharge water chemistry, precipitation, evaporation and anthropogenic sources. This is also supported by the deviation of sampling points from 1:1 line (Li et al. 2013, Wu and Sun 2016).

Evaporite dissolution

A large percentage of Na^+ and Cl^- to the groundwater come from the dissolution of evaporite (such as halite). Many groundwater sampling points fall along the 1:1 line of Na–Cl plot (Fig. 3f), signifying the dissolution of halite for high concentration of Na^+ and Cl^- (Hussin et al. 2016). A number of groundwater samples have Na^+/Cl^- ratio > 1, which inferred that Na^+ is released from weathering of feldspars such as plagioclase instead of halite dissolution (Hussin et al. 2016). In about 55% of the total groundwater samples, the value of Na^+/Cl^- ratio is more than one, indicating high contribution of Na^+ in the groundwater by hydrolysis of silicates (Subba Rao and Surya Rao 2010; Subba Rao et al. 2017).

Silicate dissolution

Sodic plagioclase mineral may be the probable source of high Na^+ over Cl^- in the study region (Eq. 3). Most groundwater sampling points plot above the equiline of bivariate graph between $HCO_3^- + SO_4^{2-}$ and $Ca^{2+} + Mg^{2+}$ (Fig. 3b), indicating the less significant role of silicate weathering than carbonate and sulphate mineral dissolution in the groundwater chemistry (Hussin et al. 2016; Adimalla and Rajitha 2018):

$$2\,Na^+[AlSi_3O_8 + 2CO_2]^- + 11H_2O$$
$$\rightarrow 2\,Na^+ + 2HCO_3^- + Al_2Si_2O_5(OH)_4 + Mg^{2+}$$
$$+ 4H_4SiO_4 \text{ Albite}$$
$$(3)$$

Ion exchange factor

As discussed earlier, the control of anions $(HCO_3^- + SO_4^{2-})$ over cations $(Ca^{2+} + Mg^{2+})$ and

the Na^+/Ca^{2+} ratio higher than unity in 55% of the total groundwater samples also verify the existence of ion exchange processes (Marghade et al. 2015; Li et al. 2018b). It is further verified by chloro-alkaline indices CAI-1 and CAI-2 proposed by Schoeller (1977).

The negative CAI index values (base ion exchange process) indicate a softening process in which exchange of Ca^{2+} and Mg^{2+} of the water with Na^+ and K^+ from the aquifer material takes place. However, in reverse ion exchange process, positive values indicate hardening process in which Na^+ and K^+ get adsorbed on the aquifer material with simultaneous release of Ca^{2+} and Mg^{2+} (Hussin et al. 2016).

The values of CAI-1 (0.44–47.05) and CAI-2 (0.26–47.06) are positive in about 85% and 99% of the total groundwater samples (Table 4), specifying that reverse ion exchange may be due to anthropogenic inputs and rainfall. In this case, cation exchange is expressed as

$$2Na^+ + CaX_2 = Ca^{2+} + 2NaX \qquad (4)$$
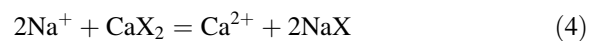
The excess of $Ca^{2+} + Mg^{2+}$ over $HCO_3^- + SO_4^{2-}$ shifts the groundwater sampling points towards the left on bivariate plot of $(Ca^{2+} + Mg^{2+})$ and $(HCO_3^- + SO_4^{2-})$, which also supports the existence of reverse ion exchange (Fig. 3b) (Marghade et al. 2015).

Anthropogenic factors

The irrigation return flow may be the source of Ca^{2+}, Mg^{2+}, Na^+, HCO_3^-, Cl^- and SO_4^{2-} in groundwater of the agricultural rural region (Subba Rao and Surya Rao 2010; Subba Rao et al. 2017). The sanitary facilities in the present region are in general poor. The strong evidence of anthropogenic perturbation is the strong positive correlation between NO_3^- and Cl^- ($r = 0.67$; Table 2), which suggests that both the ions have same source, i.e. mainly human activities (Marghade et al. 2011). However, the negative correlation between NO_3^- and HCO_3^- ($r = -0.18$) shows different sources for both the ions. NO_3^- is mainly derived from non-lithological inputs (human activities), while HCO_3^- is mainly derived from lithological inputs (soil CO_2).

In addition, the variation in TDS with other ions in groundwater indicates land use and extent of pollution (Marghade et al. 2011). Correlation of Cl^-, SO_4^{2-},

Table 4 Chloroalkaline indices

Sample no.	CAI	CAII	Sample no.	CAI	CAII	Sample no.	CAI	CAII
1	− 6.15	− 6.17	25	0.73	− 0.40	49	8.57	8.66
2	8.00	8.05	26	− 7.70	− 7.73	50	9.66	9.72
3	24.50	24.50	27	7.00	7.07	51	7.20	7.26
4	47.05	47.06	28	6.07	6.15	52	8.24	8.27
5	1.51	1.63	29	8.60	8.62	53	3.62	3.67
6	− 1.12	0.26	30	6.58	6.60	54	3.55	3.66
7	6.25	6.33	31	− 2.32	− 2.40	55	7.83	7.85
8	7.40	7.46	32	7.09	7.10	56	8.29	8.32
9	4.78	4.82	33	6.21	6.24	57	0.44	0.78
10	2.23	2.35	34	5.98	6.04	58	6.42	6.44
11	5.46	5.48	35	7.36	7.44	59	8.68	8.72
12	6.48	6.49	36	3.07	3.08	60	5.48	5.55
13	5.98	6.03	37	− 5.51	− 5.54	61	2.59	2.85
14	6.14	6.21	38	8.92	9.00	62	7.73	7.77
15	3.50	3.63	39	8.50	8.52	63	20.93	20.95
16	− 4.42	− 4.47	40	5.92	5.99	64	37.78	37.79
17	1.94	2.25	41	8.95	9.00	65	4.81	4.89
18	8.95	9.02	42	2.21	2.54	66	6.04	6.18
19	6.87	6.89	43	9.31	9.34	67	8.52	8.57
20	1.75	− 0.11	44	1.89	2.06	68	5.50	5.57
21	3.74	3.78	45	7.51	7.61	69	− 4.48	− 4.57
22	8.84	8.85	46	8.99	9.07	70	3.11	3.18
23	5.55	5.57	47	9.23	9.29	71	− 5.26	− 5.30
24	0.61	0.90	48	8.71	8.75	72	7.08	7.12

NO_3^- and Na^+ ions with TDS is used to show the impact of anthropogenic load on the aquifer chemistry (Li et al. 2016d). Pearson's correlation matrix (Table 2) showed a significant strong positive correlation between TDS and Na^+ ($r = 0.90$), NO_3^- ($r = 0.67$), Cl^- ($r = 0.95$) and SO_4^{2-} ($r = 0.80$). The strong positive correlation between TDS and Na^+ ($r = 0.90$) specifies the contribution of anthropogenic input along with silicate weathering as a cause of high level of Na^+ in groundwater (Subba Rao et al. 2017).

Geochemical modelling

Geochemical modelling of groundwater is the best method to verify the hydrochemical findings. Saturation index (SI) is a thermodynamic parameter which specifies the tendency of minerals to dissolve or precipitate during the course of water. SI is computed from activity product and equilibrium solubility of minerals (Li et al. 2010; Subba Rao 2017b),

$$\text{Where,} \quad SI = K_{IAP}/K_{SP} \tag{5}$$

K_{IAP} is ion activity product of the dissociated minerals and K_{SP} is equilibrium solubility at mineral temperature.

The saturation index (SI) for halite (NaCl), gypsum ($CaSO_4.2H_2O$), dolomite ($CaMg(CO_3)_2$), calcite ($CaCO_3$), fluorite (CaF_2), anhydrite ($CaSO_4$) and aragonite ($CaCO_3$) minerals is calculated using PHREEQC Interactive 2.13.2 software and listed in Table 5. The SI values ($− 2.76$ to $− 0.54$) are in dissolution (undersaturation) state in all the groundwater samples with respect to fluorite, whereas 64% of the total groundwater samples show calcite oversaturation (SI values: $− 0.86–1.60$). The SI results verified the contribution of carbonate dissolution in rising F^- concentrations in the groundwater by generating bulk

Table 5 Saturation indices for mineral phases

SI	Min	Max
Anhydrite	− 2.979	− 0.7404
Aragonite	− 1.0147	1.4586
Calcite	− 0.8673	1.606
Dolomite	− 1.5421	2.3065
Fluorite	− 2.7659	− 0.545
Gypsum	− 2.7419	− 0.5048
Halite	− 8.4559	− 4.6569

HCO_3^- and F^-. SI values of calcite are negative in 36% of the groundwater samples containing high fluoride concentration indicating equilibrium with respect to calcite (Magesh et al. 2016; Singh and Mukherjee 2014). The negative SI (− 8.46 to − 4.65) for halite (NaCl) is observed in the groundwater samples, indicating dissolution state resulting from the enrichment of groundwater by Na^+. About 51.4 and 64% of the total groundwater samples show oversaturation of aragonite (SI: − 1.01–1.45) and calcite (SI: − 0.86–1.60) minerals, along with oversaturation of dolomite (SI: − 1.54–2.30) in 65.3% of the total groundwater samples (Li et al. 2016d).

The groundwater shows the contribution of anhydrite in high Ca^{2+}-bearing groundwater, as it is in unsaturated state along with carbonates (SI: − 2.98 to − 0.74; Table 5). The groundwater shows a low concentration of Ca^{2+} and a high concentration of SO_4^{2-} (Table 1). This is explained by the common ion effect in which the $CaSO_4$ dissolution decreases the activity coefficient product $\gamma Ca^{2+}.\gamma CO_3^{2-}$. However, the product $(Ca^{2+})(CO_3^{2-})$ increases due to the dissolution of calcite, gypsum, aragonite and anhydrite by releasing the higher amount of Ca^{2+} in the groundwater system (Subba Rao et al. 2017). Thus, precipitation of $CaCO_3$ could occur to keep the solution in equilibrium with solid $CaCO_3$ (Subba Rao et al. 2017). Further, $CaCO_3$ precipitation becomes the crucial factor for dedolomitisation process, as discussed earlier.

Mass balance simulation analysis

Mass balance modelling is simply a hydrogeochemical simulation to calculate the extent of precipitation and mineral phase dissolving capacity, which is

widely used to uphold different weathering reactions in water–rock systems (Galego et al. 2009). It is executed with PHREEQC interactive software. In this chemical/mathematical approach, various models are generated by comparing the geochemical components at upstream with geochemical components at downstream. Simulation exemplifies the difference in concentration of the components along the flow path due to the weathering reactions (Li et al. 2007; Subba Rao et al. 2017).

On the basis of geochemical findings, calcite, dolomite, fluorite, halite, gypsum, K-feldspar, albite and anhydrite minerals are considered as the possible mineral phases for geochemical modelling simulation analysis. The existence of ion exchange reactions in the groundwater system is identified geochemically. So, CaX_2 and NaX are also incorporated in the simulation.

The mole transfer of phases is computed during simulation analysis carried out on the four flow paths listed in Table 6. Similar types of patterns are observed along all flow paths.

Simulation analysis exposes the dissolution of dolomite, gypsum, halite, K-feldspar and CO_2 along all simulated paths. The dissolution of dolomite is previously foreseen by Ca^{2+}/Mg^{2+} molar ratio (Fig. 3a). Similarly, dissolution of gypsum is foreseen by binary plot of $[(Ca^{2+}+Mg^{2+}) − 0.5\ HCO_3^-]$ versus SO_4^{2-} and plot of Ca^{2+} and versus SO_4^{2-} verified by positive values (Figs. 3d) calculated for gypsum phase by simulation analysis. The negative values (− 0.00,601, − 0.000045, − 0.00226) for calcite confirm the precipitation of calcite predicted by the plot of SI of gypsum against dolomite and ion exchange process (Subba Rao et al. 2017). The gypsum dissolution elevates the concentration of Ca^{2+}, while the anhydrite decreases the concentration of Ca^{2+} due to its precipitation. The binary plot of Na–Cl (Fig. 3f) and Na^+ versus TC forecasted the dissolution of halite (Fig. 3g), which is verified by the positive values (Table 6) of mass transfer for halite phase in the groundwater body. The possible sources for K^+ are weathering of K-feldspars present and application of potash fertilisers. A positive value (Table 6) of mineral mass balance for K-feldspars indicates that the feldspars are in dissolution state.

The positive values (Table 6) of simulation for CO_2 (g) signify the contribution of dissolution of soil CO_2

Table 6 Mineral phase transfer amount

Phases	Chemical expression	Simulation path			
		Model I Samples 8–11	Model II Samples 37–57	Model III Sample no. 21–26	Model IV Sample no. 31–33
Calcite	$CaCO_3$	− 0.00601	− 0.000045	− 0.00226	0.0022
CaX_2	CaX_2	− 0.00664	− 0.000313	− 0.000075	− 0.0032
Dolomite	$CaMg(CO_3)_2$	0.00433	0.001301	0.002552	0.00030
Halite	$NaCl$	0.01857	0.002105	0.0043	0.008416
Gypsum	$CaSO_4:2H_2O$	27.7600	27.7500	27.75	27.75
K-feldspar	$KAlSi_3O_8$	0.00136	0.000947	0.00126	0.001152
NaX	NaX	− 0.0133	0.000626	0.000015	0.0064
Albite	$NaAlSi_3O_8$	− 0.00136	− 0.000947	− 0.00126	− 0.00115
Anhydrite	$CaSO_4$	− 27.76000	− 27.7500	− 27.75	− 27.75
$CO_2(g)$	CO_2	0.00445	0.00278	0.00369	0.00293

in increasing the HCO_3^- concentration in the groundwater. The precipitation of calcite (along first three flow paths) and anhydrite is predicted by their negative simulation values (Table 6). Inclusively, the dolomite and gypsum dissolution increases the concentration of Ca^{2+}, while the calcite and anhydrite precipitation and cation exchange reduce the concentration of Ca^{2+} simultaneously with the increase of Na^+ in the groundwater. The dissolution of calcite in Model IV is supported by the positive value (0.0022) of CaX_2 phase, indicating the role of ion exchange in chemical load of groundwater system. The negative values (− 0.000313, − 0.000075, − 0.0032) for CaX_2 phase and positive values (0.000626, 0.000015, 0.0064) for NaX phase in model II, III and IV authenticated the presence of ion exchange foreseen by chloro-alkaline indices and $(Ca^{2+} + Mg^{2+})$ and $(HCO_3^- + SO_4^{2-})$ bivariate plot (Fig. 3b). During this process, Na^+ released by the dissolution of halite underwent exchange with Ca^{2+} absorbed on the rock surface.

It is found that the concentration of Na^+ in the groundwater has increased by cation exchange, while precipitation of albite (negative values of simulation) lowers its concentration (Table 6). A very small amount of CO_2 dissolved in flow path III (21–26) is due to coal deposits present in Barakar Formation of Gondwana Supergroup of Permo-Carboniferous age and continuous recharging responsible for the precipitation of fluorite.

Therefore, the simulation analysis of groundwater (Models I to IV) substantiates the water–rock interactions as the main parameters responsible for chemical

characterisation of groundwater. In addition, the dry climate and man-made activities affect the rate of reaction and intensity (Li et al. 2016b).

Principal component analysis

The principal component analysis (PCA) with varimax-rotated R-mode was computed on the 72 set of 12 water parameters, such as pH, EC, TDS, Na^+, K^+, Ca^{2+}, Mg^{2+}, HCO_3^-, Cl^-, F^-, NO_3^- and SO_4^{2-}. According to Kaiser criterion (Wu and Sun 2016), only those principal components (PCs) are extracted with rotation of loadings for the maximum variance, which have eigenvalues larger than one.

The high positive loading of EC, TDS, Na^+, K^+, Ca^{2+}, Cl^-, NO_3^- and SO_4^{2-} in the first PC accounts for 49.37% of the total variance (Table 7). As discussed, significant positive correlation ($r = 0.9, 0.78, 0.95$ and 0.67) is observed between TDS and Na^+ (Table 2), which signifies the contribution of these ions in governing the hydrochemical characteristics of groundwater. A very high positive PC loading of TDS (0.99) and Cl^- (0.95) signifies the impact of anthropogenic loading on hydrochemistry of groundwater. Strong positive correlation between Na^+ with Cl ($r = 0.81$) and SO_4^{2-} ($r = 0.80$) indicates high pollution level of groundwater (Barzegar et al. 2017; Subba Rao and Chaudhary 2019). The high content of Na^+ (0.84) signifies the role of geogenic and anthropogenic sources for high concentration of Na^+ in the groundwater (Marghade et al. 2015, Isa et al. 2017).

Table 7 Principal component loadings

Parameters	PC1	PC2	PC3
pH	− 0.20	0.10	**− 0.80**
EC	**0.88**	0.19	0.02
TDS	**0.99**	0.12	0.01
Na^+	**0.84**	0.32	− 0.23
K^+	**0.61**	0.18	− 0.01
Ca^{2+}	**0.80**	− 0.11	0.34
Mg^{2+}	0.46	− 0.47	0.30
HCO_3^-	0.28	**0.86**	0.04
Cl^-	**0.95**	− 0.06	− 0.05
SO_4^{2-}	**0.75**	**0.54**	− 0.01
NO_3^-	**0.72**	**− 0.51**	0.25
F^-	0.21	− 0.04	**− 0.87**
Eigenvalue	5.92	2.11	1.23
% Total variance	49.37	17.59	10.30
Cumulative eigenvalue	5.92	8.03	9.27
Cumulative %	49.37	66.96	77.27

Bold numbers indicates strong positive correlation between two parameters

Na^+/Cl^- ratio greater than one signifies silicate dissolution. The secondary salt precipitation due to irrigation return flows, elevated rate of evaporation and anthropogenic inputs are mainly governing the concentration of Cl^- (Subba Rao 2017a). The significant positive correlation between Na^+ and Cl^- ($r = 0.81$) and SO_4^{2-} ($r = 0.80$), between Ca^{2+} and Cl^- ($r = 0.75$) and NO_3^- ($r = 0.72$) supports the role of anthropogenic input over rock mineral interactions (Aksever and Buyuksahin 2017). The main sources of K^+ in the study area are the weathering of feldspars and potash fertilisers. The plot of ($Ca^{2+} + Mg^{2+}$) versus ($HCO_3^- + SO_4^{2-}$) (Fig. 3b) strongly supports the presence of reverse ion exchange in the study area (Marghade et al. 2015). The less significant positive correlation between Na^+ and Ca^{2+} which makes Na^+/Cl^- ratio greater than one further strongly supports the existence of reverse ion exchange, which is further strengthened by first principal loading (Sudheer Kumar et al. 2017). A low dissolution of Mg^{2+} and Ca^{2+} ions due to the precipitation of calcite is indicated by negative PC scores in the first PC of 46 groundwater samples. Therefore, PC-1 reveals the silicate weathering and reverse ion exchange followed by human activities as the contamination sources.

The second PC endorses the 17.59% of the total variance with high positive loading of HCO_3^- and SO_4^{2-} as well as high negative loading of NO_3^-. The significant correlation between HCO_3^- and SO_4^{2-} ($r = 0.62$; Table 2) indicates the common source of these ions. The negative correlation between HCO_3^- and NO_3^- ($r = − 0.18$) signifies the different sources of these ions (Marghade et al. 2012). This again supports the fact that calcite dissolution is the main process governing HCO_3^- content. Non-geogenic sources are responsible for high nitrate content (Wu and Sun 2016). Thus, the second PC is assumed to be an indicative of influence of soil CO_2 and soil amendment of gypsum (Wagh et al. 2017). The PC1 and PC2 (Table 7) shows high positive loadings (3.37, 5.80) for groundwater sampling point 31, which has the highest concentration of Ca^{2+} (364 mg/L), HCO_3^- (1159 mg/L) and SO_4^{2-} (925 mg/L). This suggests that the geogenic sources are masked by anthropogenic sources and reverse ion exchange in the groundwater.

The third PC accounts for 10.3% of the total variance, where pH (-0.80) and F^- (0.87) show strong negative weights (Table 7). The pH has a low positive correlation with F^- ($r = 0.43$; Table 2). The high HCO_3^- content in alkaline water (pH: 6.7–8.6) accelerates the dissolution of F^- in groundwater (Subba Rao 2013, 2018). Simultaneously, negative correlation of F^- with Ca^{2+} and Mg^{2+} indicates the precipitation of calcite that is reduction in Ca^{2+} content, which supports the dissolution of F^- in the groundwater. Only 12% of the total groundwater sampling points have F^- content above 1.5 mg/L due to the reverse ion exchange process. Thus, the third PC is assumed to be an indicative of F^- loading in the groundwater (Table 7).

Conclusions

The application of statistical, geochemical and multivariate approaches gives an insight of hydrogeochemistry of groundwater to assess the groundwater quality from semi-arid Wani region of eastern Maharashtra, India. The main conclusions drawn are as follows:

- Groundwater shows high concentrations of Na^+ and HCO_3^- ions. A strong correlation of Na^+ with

Cl^-, SO_4^{2-} and NO_3^- indicates the high pollution level of groundwater. Negative ion exchange between F^- and Ca^{2+} and positive correlation between F^- and Na^+ support the acceleration of F^- content in the groundwater. The precipitation of calcite and the dissolution of dolomite cause the dedolomitisation process in the study region. The positive CA1 and CA2, bivariate plots [$(Ca^{2+} + Mg^{2+})$ and $(HCO_3^- + SO_4^{2-})$ indicate the reverse ion exchange, depending upon the groundwater flow path and residence time conditions. The strong relation of TDS with Cl^-, SO_4^{2-}, NO_3^- and Na^+ ions is strongly reinforced the impact of human activities on the groundwater chemistry.

- The health risks assessment showed the higher percentage of health risk among children (40%) on consumption of F^--polluted groundwater than that for adults (23%) in the study region.

- Geochemical modelling of data supports the rock weathering reactions (calcite dissolution, dolomite dissolution, gypsum dissolution, oversaturation of aragonite, $CaCO_3$ precipitation and dedolomitisation) taking place in the present study region.

- Principal component analysis extracted a three-factor model. The high positive loading of PC1 (EC, TDS, Na^+, K^+, Ca^{2+}, Cl^-, NO_3^- and SO_4^{2-}) represents the carbonate weathering, silicate dissolution and ion exchange process by anthropogenic activities; PC2 (HCO_3^- and SO_4) indicates the contribution of soil CO_2 and human activities, and PC3 (F^-) reveals the dissolution of fluorite by the precipitation of $CaCO_3$.

- The present study suggests the control of anthropogenic activities (wastes disposal and excessive use of agrochemicals) to prevent the contamination of groundwater resources. Regular groundwater quality monitoring stations are necessary. Creation of public awareness is essential for effective groundwater management. The study recommends that the rainwater harvesting techniques like surface water storage, recharge pits, check dams, etc., should be followed to improve the groundwater quality as per drinking water quality standards as well as to augment the groundwater levels which are the best methods for sustainable development and management of groundwater resources.

References

Adimallaa, N., & Qian, H. (2019). Groundwater quality evaluation using water quality index (WQI) for drinking purposes and human health risk (HHR) assessment in an agricultural region of Nanganur, south India. *Ecotoxicology and Environmental Safety, 176,* 153–161.

Adimallaa, N., & Rajitha, S. (2018). Spatial distribution and seasonal variation in fluoride enrichment in groundwater and its associated human health risk assessment in Telangana State, South India. *Human and Ecological Risk Assessment.* https://doi.org/10.1080/10807039.2018.143817.

Adimallaa, N., Sathish Kumar, V., Li, P., et al. (2018). Evaluation of groundwater quality, Peddavagu in Central Telangana (PCT), South India: An insight of controlling factors of fluoride Enrichment. *Modeling Earth Systems and Environment.* https://doi.org/10.1007/s40808-018-0443-z.

Aksever, F., & Buyuksahin, S. (2017). Assessment of variations in water quality using statistical techniques: A case study of Isiklilake, Civril/Denizli, Turkey. *Arabian Journal of Geosciences, 10,* 1–17.

American Public Health Association (APHA). (1999). *Standard methods for the examination of water and wastewater* (20th ed., p. 1268). Washington DC: APHA.

Anand, B., Karunanidhi, D., Subramani, T., Srinivasamoorthy, K., Suresh, M., et al. (2019). Long-term trend detection and spatiotemporal analysis of groundwater levels using GIS techniques in Lower Bhavani River basin, Tamil Nadu, India. *Environment, Development and Sustainability.* https://doi.org/10.1007/s10668-019-00318-3.

Aravinthasamy, P., Karunanidhi, D., Subramani, T., Srinivasamoorthy, K., Anand, B., et al. (2019). Geochemical evaluation of fluoride contamination in groundwater from Shanmuganadhi River basin, South India: Implication on human health. *Environmental Geochemistry and Health.* https://doi.org/10.1007/s10653-019-00452-x.

Barzegar, R., Moghaddam, A. A., Tziritis, E., Fakhri, M. S., Soltani, S., et al. (2017). Identification of hydrogeochemical processes and pollution sources of groundwater resources in the Marand Plain, northwest of Iran. *Environmental Earth Sciences, 76,* 297.

Brindha, K., & Elango, L. (2013). Geochemistry of fluoride rich groundwater in a weathered granitic rock region, Southern India. *Water Quality, Exposure and Health, 5*(3), 127–138.

Brindha, K., Jagadeshan, G., Kalpana, L., Elango, L., et al. (2016). Fluoride in weathered rock aquifers of Southern India: Managed aquifer recharge for mitigation. *Environmental Science and Pollution Research, 23*(9), 8302–8316.

CGWB. (2013). Ground Water Information Yavatmal District Maharashtra, 1790/DBR/2013. http://www.cgwb.gov.in/District_Profile/Maharashtra/Yavatmal.pdf.

Duraisamy, S., Govindhaswamy, V., Duraisamy, K., Krishinaraj, S., Balasubramanian, A., Thirumalaisamy, S., et al. (2018). Hydrogeochemical characterization and evaluation of groundwater quality in Kangayam taluk, Tirupur district, Tamil Nadu, India, using GIS techniques. *Environmental Geochemistry and Health.* https://doi.org/10.1007/s10653-018-0183-z.

Fijani, E., Moghaddam, A. A., Frank, T., Tsai, C., Tayfur, G., et al. (2017). Analysis and Assessment of Hydrochemical Characteristics of Maragheh-Bonab Plain Aquifer, Northwest of Iran. *Water Resources Management, 31,* 765–780.

Freeze, R. A., & Cherry, J. A. (1979). *Groundwater* (p. 603). New Jersey: Prentice-Hall.

Galego, F. P., Carreira, P. M., Bahir, M., et al. (2009). Mass balance simulation and principal components analysis applied to groundwater resources: Essaouira basin (Morocco). *Environmental Earth Sciences, 1,* 2. https://doi.org/10.1007/s12665-009-0133-2.

He, S., & Wu, J. (2019). Hydrogeochemical characteristics, groundwater quality and health risks from hexavalent chromium and nitrate in groundwater of Huanhe Formation in Wuqi County, northwest China. *Exposure and Health, 11*(2), 125–137. https://doi.org/10.1007/s12403-018-0289-7.

He, X., Wu, J., He, S., et al. (2019). Hydrochemical characteristics and quality evaluation of groundwater in terms of health risks in Luohe aquifer in Wuqi County of the Chinese Loess Plateau, northwest China. *Human and Ecological Risk Assessment, 25*(1–2), 32–51. https://doi.org/10.1080/10807039.2018.1531693.

Hussin, N. H., Yusoff, I., Tahir, W., Mohamed, I., Ibrahim, A. I. N., Rambli, A., et al. (2016). Multivariate statistical analysis for identifying water quality and hydrogeochemical evolution of shallow groundwater in Quaternary deposits in the Lower Kelantan River Basin, Malaysian Peninsula. *Environmental Earth Sciences, 75,* 1081. https://doi.org/10.1007/s12665-016-5705-3.

Isa, N. M., Aris, A. Z., Narany, T. S., Sulaiman, W. N. A., et al. (2017). Applying the scores of multivariate statistical analyses to characterize the relationships between the hydrochemical properties and groundwater conditions in respect of the monsoon variation in Kapas Island, Terengganu, Malaysia. *Environmental Earth Sciences, 76,* 169.

Karunanidhi, D., Aravinthasamy, P., Subramani, T., Wu, J., et al. (2019). SrinivasamoorthyK. Potential health risk assessment for fluoride and nitrate contamination in hard rock aquifers of Shanmuganadhi River basin, South India. *Human and Ecological Risk Assessment, 25*(1–2), 250–270. https://doi.org/10.1080/10807039.2019.1568859.

Karunanidhi, D., Vennila, G., Suresh, M., Rangarajan, R., et al. (2014). Groundwater investigation and possible zones identification through Schlumberger resistivity data using GIS tools in Omalur taluk, Salem District, Tamil Nadu, India. *Indian Journal of Geo-Marine Sciences, 43*(4), 542–553.

Karunanidhi, D., Vennila, G., Suresh, M., Subramanian, S. K., et al. (2013). Evaluation of the groundwater quality feasibility zones for irrigational purposes through GIS in Omalur Taluk, Salem District, South India. *Environmental Science and Pollution Research, 20*(10), 7320–7333. https://doi.org/10.1007/s11356-013-1746-2.

Kshetrimayum, K. S. (2015). Hydrochemical evaluation of shallow groundwater aquifers: A case study from a semi-arid Himalayan foothill river basin, northwest India. *Environmental Earth Sciences, 74*(10), 1–14. https://doi.org/10.1007/s12665-015-4697-8.

Li, P., He, X., Li, Y., Xiang, G., et al. (2019a). Occurrence and health implication of fluoride in groundwater of loess aquifer in the Chinese Loess Plateau: A case study of Tongchuan, Northwest China. *Exposure and Health, 11*(2), 95–107. https://doi.org/10.1007/s12403-018-0278-x.

Li, P., He, S., Yang, N., Xiang, G., et al. (2018a). Groundwater quality assessment for domestic and agricultural purposes in Yan'an City, northwest China: Implications to sustainable groundwater quality management on the Loess Plateau. *Environmental Earth Sciences, 77*(23), 775. https://doi.org/10.1007/s12665-2018-7968-3.

Li, P., Li, X., Meng, X., Li, M., Zhang, Y., et al. (2016a). Appraising groundwater quality and health risks from contamination in a semiarid region of northwest China. *Exposure and Health, 8*(3), 361–379. https://doi.org/10.1007/s12403-016-0205-y.

Li, P., Qian, H., Wu, J., Ding, J., et al. (2010). Geochemical modeling of groundwater in southern plain area of Pengyang County, Ningxia, China. *Water Science and Engineering, 3*(3), 282–291. https://doi.org/10.3882/j.issn.1674-2370.2010.03.004.

Li, P., Tian, R., Liu, R., et al. (2019b). Solute geochemistry and multivariate analysis of water quality in the Guohua phosphorite mine, Guizhou Province, China. *Exposure and Health, 11*(2), 81–94. https://doi.org/10.1007/s12403-018-0277-y.

Li, P., Tian, R., Xue, C., Wu, J., et al. (2017). Progress, opportunities and key fields for groundwater quality research under the impacts of human activities in China with a special focus on western China. *Environmental Science and Pollution Research, 24*(15), 13224–13234. https://doi.org/10.1007/s11356-017-8753-7.

Li, P., Wu, J., Qian, H., Zhang, Y., Yang, N., Jing, L., et al. (2016b). Hydrogeochemical characterization of groundwater in and around a wastewater irrigated forest in the southeastern edge of the Tengger Desert, Northwest China. *Exposure and Health, 8*(3), 331–348. https://doi.org/10.1007/s12403-016-0193-y.

Li, P., Wu, J., Qian, H., et al. (2016c). Hydrochemical appraisal of groundwater quality for drinking and irrigation purposes and the major influencing factors: A case study in and around Hua County, China. *Arabian Journal of Geosciences, 9*(1), 15. https://doi.org/10.1007/s12517-015-2059-1.

Li, P., Wu, J., Tian, R., He, S., He, X., Xue, C., et al. (2018b). Geochemistry, hydraulic connectivity and quality appraisal of multilayered groundwater in the Hongdunzi Coal Mine, Northwest China. *Mine Water and the Environment, 37*(2), 222–237. https://doi.org/10.1007/s10230-017-0507-8.

Li, P., Zhang, Y., Yang, N., Jing, L., Yu, P., et al. (2016d). Major ion chemistry and quality assessment of groundwater in and around a mountainous tourist town of China. *Exposure and Health, 8*(2), 239–252. https://doi.org/10.1007/s12403-016-0198-6.

Li, P. Y., Qian, H., Wu, J. H., Zhang, Y. Q., Zhang, H. B., et al. (2013). Major ion chemistry of shallow groundwater in the Dongsheng Coalfield, Ordos Basin, China. *Mine Water and the Environment, 32,* 195–206. https://doi.org/10.1007/s10230-013-0234-8.

Li, Y., Wang, J., Wu, Y., Xu, Z., Fu, X., Hou, G., et al. (2007). Mass balance simulation and its application to refining flow

field in Binchang area, China. *Environmental Geology,* *52*(4), 739–745.

Magesh, N. S., Chandrasekar, N., Elango, L., et al. (2016). Occurrence and distribution of fluoride in the groundwater of the Tamiraparani River basin, South India: A geostatistical modeling approach. *Environmental Earth Sciences,* *75,* 1483. https://doi.org/10.1007/s12665-016-6293-y.

Marghade, D., Malpe, D. B., Subbarao, N., Sunitha, B., et al. (2019). Geochemical assessment of fluoride enriched groundwater and health implications from a part of Yavtmal District. *India. Human and Ecological Risk Assessment*. https://doi.org/10.1080/10807039.2018.1528862.

Marghade, D., Malpe, D. B., Subbarao, N., et al. (2015). Identification of controlling processes of groundwater quality in a developing urban area using principal component analysis. *Environmental Earth Sciences,* *74,* 5919–5933. https://doi.org/10.1007/s12665-015-4616-z.

Marghade, D., Malpe, D. B., Zade, A. B., et al. (2010). Assessment of groundwater quality in landfill area of Nagpur city, central India. *Journal of Environmental Hydrology,* *18*(18), 1–12.

Marghade, D., Malpe, D. B., Zade, A. B., et al. (2011). Geochemical characterization of groundwater from northeastern part of Nagpur urban, Central India. *Environmental Earth Sciences,* *62,* 1419–1430.

Marghade, D., Malpe, D. B., Zade, A. B., et al. (2012). Major ion chemistry of shallow groundwater of a fast-growing city of Central India. *Environmental Monitoring and Assessment,* *184,* 2405–2418.

Nagaraju, A., Sharifi, Z., Balaji, E., et al. (2016). Statistical and analytical evaluation of groundwater quality of Tirupati area, Chittoor District, A.P, South India. *Journal of the Geological Society of India,* *88,* 222–234.

Piper, A. M. (1944). A graphical procedure in the geochemical interpretation of water analysis. *Transactions American Geophysical Union,* *25,* 914–928.

Rina Kumar, P., Datta, S., Rao, M. S., Mukherjee, S., Azad, C., et al. (2018). Anthropogenic perturbations induced groundwater vulnerability to pollution in the industrial Faridabad District, Haryana, India. *Environmental Earth Sciences,* *77,* 187.

Schoeller, H. (1977). Geochemistry of groundwater. In Brown, R.H., Konoplyantsev, A.A., Ineson, J., & Kovalevsky, V.S. (eds.) *Groundwater studies—an international guide for research and practice*, Chap. 15, UNESCO, Paris, 1–18.

Selvam, S. (2014). Irrigational feasibility of groundwater and evaluation of hydrochemistry facies in the SIPCOT industrial area, South Tamilnadu, India: A GIS approach. *Water Quality, Exposure and Health*. https://doi.org/10.1007/s12403-014-0146-2.

Singaraja, C., Chidambaram, S., Prasanna, M. V., Thivya, C., Thilagavathi, R., et al. (2014). Statistical analysis of the hydrochemical evolution of groundwater in hard rock coastal aquifers of Thoothukudi district in Tamil Nadu, India. *Environmental Earth Sciences,* *71*(1), 451–464.

Singh, C. K., & Mukherjee, S. (2014). Aqueous geochemistry of fluoride enriched groundwater in arid part of Western India. *Environmental Science and Pollution Research,* *22*(4), 2668–2678.

Sreedevi, P. D., Sreekanth, P. D., Ahmed, S., Reddy, D. V., et al. (2018). Appraisal of groundwater quality in a crystalline

aquifer: A chemometric approach. *Arabian Journal of Geosciences*. https://doi.org/10.1007/s12517-018-3480-z.

Subba Rao, N. (2003). Groundwater quality: Focus on fluoride concentration in rural parts of Guntur District, Andhra Pradesh, India. *Hydrological Sciences Journal,* *48,* 835–847.

Subba Rao, N. (2006). Seasonal variation of groundwater quality in a part of Guntur District, Andhra Pradesh, India. *Environmental Geology,* *49,* 413–429.

Subba Rao, N. (2011). High-fluoride groundwater. *Environmental Monitoring and Assessment,* *176,* 637–645.

Subba Rao, N. (2017a). Controlling factors of fluoride in groundwater in a part of South India. *Arabian Journal of Geosciences*. https://doi.org/10.1007/s12517-017-3291-7.

Subba Rao, N. (2017b). Hydrogeology: Problems with Solutions Andhra Pradesh, India. *Environmental Geology,* *49,* 413–429.

Subba Rao, N. (2017c). Controlling factors of fluoride in groundwater in a part of South India. *Arabian Journal of Geosciences*. https://doi.org/10.1007/s12517-017-3291-7.

Subba Rao, N. (2018). Groundwater quality from a part of Prakasam district, Andhra Pradesh, India. *Appl Water Sci.,* *80,* 30. https://doi.org/10.1007/s13201-018-0665-2.

Subba Rao, N., & Chaudhary, M. (2019). Hydrogeochemical processes regulating the spatial distribution of groundwater contamination, using pollution index of groundwater (*PIG*) and hierarchical cluster analysis (HCA): A case study. *Groundwater for Sustainable Development*. https://doi.org/10.1016/j.gsd.2019.100238.

Subba Rao, N., Marghade, Deepali, Dinakar, A., Chandana, I., Sunitha, B., Ravindra, B., et al. (2017). Geochemical characteristics and controlling factors of chemical composition of groundwater in a part of Guntur district, Andhra Pradesh, India. *Environmental Earth Sciences,* *76,* 747. https://doi.org/10.1007/s12665-017-7093-8.

Subba Rao, N., Srihari, B., Spandana, D., Sravanthi, M., Kamalesh, T., Abraham Jayadeep, V., et al. (2019a). Comprehensive understanding of groundwater quality and hydrogeochemistry for the sustainable development of suburban area of Visakhapatnam, Andhra Pradesh, India. *Human and Ecological risk Assessment,* *10*(1080/10807039), 1571403.

Subba Rao, N., Subrahmanyam, A., Babu Rao, G., et al. (2013). Fluoride-bearing groundwater in Gummanampadu Sub-basin, Guntur District, Andhra Pradesh, India. *Environmental Earth Sciences,* *70,* 575–586.

Subba Rao, N., Sunitha, B., Adimalla, N., Chaudhary, M., et al. (2019b). Quality criteria for groundwater use from a rural part of Wanaparthy District, Telangana State, India, through ionic spatial distribution (ISD), entropy water quality index (EWQI) and principal component analysis (PCA). *Environmental Geochemistry and Health*. https://doi.org/10.1007/s10653-019-00393-5.

Subba Rao, N., & Surya Rao, P. (2010). Major ion chemistry of groundwater in a river basin: A study from India. *Environmental Earth Sciences,* *61,* 757–775.

Sudheer Kumar, M., Dhakate, R., Yadagiri, G., Srinivasa Reddy, K., et al. (2017). Principal component and multivariate statistical approach for evaluation of hydrochemical characterization of fluoride-rich groundwater of

ShaslarVaru watershed, Nalgonda District, India. *Arabian Journal of Geosciences, 10*(4), 1–17.

Tay, C. K., Hayford, E. K., Hodgsoni, I. O. A., et al. (2017). Application of multivariate statistical technique for hydrogeochemical assessment of groundwater within the Lower Pra Basin, Ghana. *Applied Water Science, 7,* 1131–11150.

Thilagavathi, N., Subramani, T., Suresh, M., Karunanidhi, D., et al. (2015). Mapping of groundwater potential zones in Salem Chalk Hills, Tamil Nadu, India, using remote sensing and GIS techniques. *Environmental Monitoring and Assessment*. https://doi.org/10.1007/s10661-015-4376-y.

USEPA. (2004). Risk Assessment Guidance for Superfund Volume I: *Human Health Evaluation Manual* (Part E). http://www.epa.gov/oswer/riskassessment/ragse/pdf/introduction.pdf.

Wagh, V. M., Panaskar, D. B., Muley, A. A., et al. (2017). Estimation of nitrate concentration in groundwater of Kadava river basin-Nashik district, Maharashtra, India by using artificial neural network model. *Modeling Earth Systems and Environment*. https://doi.org/10.1007/s40808-017-0290-3.

WHO. (2011). *Guidelines for drinking-water quality* (4th ed.). Geneva: World Health Organization.

Wu, J., Li, P., Qian, H., Duan, Z., Zhang, X., et al. (2014). Using correlation and multivariate statistical analysis to identify hydrogeochemical processes affecting the major ion chemistry of waters: Case study in Laoheba phosphorite mine in Sichuan, China. *Arabian Journal of Geosciences, 7*(10), 3973–3982. https://doi.org/10.1007/s12517-013-1057-4.

Wu, J., Li, P., Wang, D., Ren, X., Wei, M., et al. (2019a). Statistical and multivariate statistical techniques to trace the sources and affecting factors of groundwater pollution in a rapidly growing city on the Chinese Loess Plateau. *Human and Ecological Risk Assessment*. https://doi.org/10.1080/10807039.2019.1594156.

Wu, J., & Sun, Z. (2016). Evaluation of shallow groundwater contamination and associated human health risk in an alluvial plain impacted by agricultural and industrial activities, mid-west China. *Expo Health, 8*(3), 311–329.

Wu, J., Zhou, H., He, S., Zhang, Y., et al. (2019b). Comprehensive understanding of groundwater quality for domestic and agricultural purposes in terms of health risks in a coal mine area of the Ordos basin, north of the Chinese Loess Plateau. *Environmental Earth Sciences, 78*(15), 446. https://doi.org/10.1007/s12665-019-8471-1.